Journal of Crystal Growth 312 (2010) 3034–3039

Contents lists available at ScienceDirect

Journal of Crystal Growth

journal homepage: www.elsevier.com/locate/jcrysgro

Effect of Mn concentration and growth temperature on nanostructures and magnetic properties of $Ge_{1-x}Mn_x$ grown on Si

Ya Wang [a], Faxian Xiu [b], Yong Wang [a,*], Hongyi Xu [a], De Li [a], Xufeng Kou [b], Kang L. Wang [b], Ajey P. Jacob [c], Jin Zou [a,d,*]

[a] Materials Engineering, The University of Queensland, Brisbane QLD 4072, Australia
[b] Device Research Laboratory, Electrical Engineering, University of California at Los Angeles, CA 90095, USA
[c] Intel assignee to Western Institute of Nanoelectronics (WIN) Intel Corporation, 2200 Mission College Blvd, Santa Clara, CA 95052, USA
[d] Centre for Microscopy and Microanalysis, The University of Queensland, Brisbane QLD 4072, Australia

ARTICLE INFO

Article history:
Received 14 June 2010
Received in revised form
30 June 2010
Accepted 8 July 2010
Communicated by H. Asahi
Available online 13 July 2010

Keywords:
A3. Molecular beam epitaxy
B2. Magnetic materials
B2. Semiconducting germanium

ABSTRACT

The nanostructures and magnetic properties of $Ge_{1-x}Mn_x$ thin films grown on Si substrates by molecular beam epitaxy, with different nominal Mn concentrations (1–4%) and different growth temperatures, have been systematically investigated by transmission electron microscopy and superconducting quantum interference device. It was discovered that when $Ge_{1-x}Mn_x$ thin films were grown at 70 °C, with increase in Mn concentration, Mn-rich tadpole shaped clusters started to nucleate at 1% Mn and become dominate in the entire film at 4% Mn. While for the thin films grown at 150 °C, tadpoles was firstly seen in the film with 1% Mn and subsequently Mn-rich secondary precipitates became dominant. The magnetic properties show specific features, which are mainly related to the nature and amount of Mn-rich clusters/precipitates within these thin films.

1. Introduction

Due to the promising applications in future spintronic devices, diluted magnetic semiconductors (DMS) have attracted enormous attention in the past few decades [1–3]. Compared with other DMSs, GeMn DMS becomes more attractive in terms of compatibility with current Si technology and easy commercialization. [4–8] In this regard, the ultimate goal is to obtain a high-quality GeMn DMS, which can function well above room temperature. Unfortunately, secondary precipitates such as Mn_5Ge_3 [9–11] and $Mn_{11}Ge_8$, [12] or other Mn-rich clusters, [13–16] caused by low Mn solubility in Ge, make it a challenging task to achieve. As a matter of fact, such precipitates/clusters are commonly observed in Mn-doped Ge, no matter whether the materials were grown by the dedicated molecular beam epitaxy (MBE) facility, [16–18] the well-established ion beam implantation techniques, [19] or the Bridgman's crystal growth technique. [20] For example, Ayoub et al. [5] revealed Mn_5Ge_3 precipitates in diluted GeMn epitaxial films with 3.3% Mn grown by MBE. Our previous study [12] confirmed the $Mn_{11}Ge_8$ in the GeMn films with 4% Mn grown by MBE. Likewise, Passacantando et al. [19] found Ge_3Mn_5 clusters in Mn+ implanted Ge single crystals, and $Mn_{11}Ge_8$ was reported in GeMn single crystals prepared by the Bridgman's technique [20]. On the other hand, growth temperature, an important factor affecting the structure and magnetic properties of GeMn DMS, has been extensively investigated. [6,9,21] Devillers et al. [6] studied GeMn thin films grown at different temperatures ranging from 80 to 200 °C, and revealed at least four different Mn-rich clusters, including nanocolumns and Ge_3Mn_5 precipitates. In another study, Ahlers et al. [9] investigated GeMn thin films with 5% Mn grown at 60–120 °C and they found that nano-sized Ge_3Mn_5 can be observed for samples grown at substrate temperature $T_s \geq 70$ °C with 5% Mn and precipitate-free samples can be acquired at $T_s = 60$ °C. Nevertheless, these studies were mainly focused on GeMn thin films grown on Ge substrates, and little attention has been paid for these novel thin films grown on the Si substrate [10,11], although such information is essential for such a system to be combined with the matured Si technology.

In this study, through detailed investigations by transmission electron microscopy (TEM) and superconducting quantum interference device investigations (SQUID), the effect of Mn concentration and growth temperature on structural and magnetic properties of GeMn thin films grown on Si are comprehensively investigated. Moreover, coherent interface between the secondary $Mn_{11}Ge_8$ precipitates and the Ge matrix was firstly witnessed.

2. Experiment details

The $Ge_{1-x}Mn_x$ thin films with different nominal Mn concentrations (namely, $x = 0.01$, 0.02, 0.03 and 0.04, respectively) were

* Corresponding authors.
E-mail addresses: y.wang4@uq.edu.au (Y. Wang), j.zou@uq.edu.au (J. Zou).

0022-0248/$ - see front matter © 2010 Elsevier B.V. All rights reserved.
doi:10.1016/j.jcrysgro.2010.07.008

grown on Si (0 0 1) substrates at 70 and 150 °C using a Perkin-Elmer solid source MBE system. The Si substrates were cleaned by H_2SO_4:H_2O_2 (5:3) and 10% HF with a final step of HF etching. Native oxide was removed by 800 °C annealing for 10 min in vacuum. During the growth, a nominal 35 nm thick Ge buffer layer was firstly deposited on Si (0 0 1) substrates at 400 °C. After that, Mn-doped Ge was deposited on the top of Ge buffer layer at 70 and 150 °C. The Ge growth rate was set to be 0.02 nm/s. To simplify, a shortened term is used to distinguish sample states hereafter. For example, S70-1 refers to the $Ge_{1-x}Mn_x$ thin film with $x=0.01$ grown at 70 °C. TEM, high resolution TEM (HRTEM) and energy dispersive X-ray spectroscopy (EDS) were employed to investigate the structural and chemical characteristics of grown thin films. Cross-sectional TEM specimens were prepared by mechanically polished using a tripod technique, followed by a final thinning using a Gatan precision ion polishing system. The HRTEM and EDS experiments were conducted in a Philips Tecnai F20 TEM, operating at 200 kV.

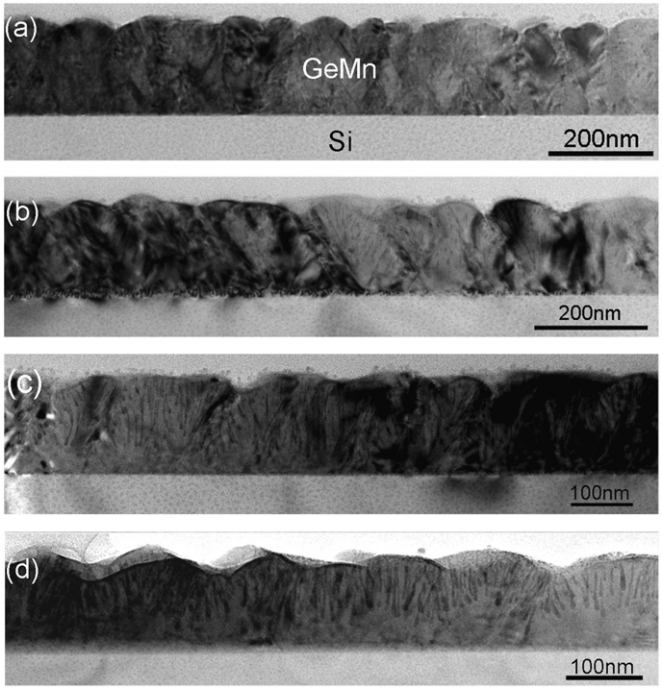

Fig. 1. Typical cross-sectional TEM images of samples grown at 70 °C: S70-1 (a), S70-2 (b), S70-3 (c) and S70-4 (d).

3. Results and discussion

3.1. Structural properties

Fig. 1(a)–(d) are typical cross-sectional TEM images of S70-1, S70-2, S70-3, and S70-4, respectively, and show their general morphology of grown $Ge_{1-x}Mn_x$ thin films. In all cases, rough surfaces can be observed. By carefully examining the $Ge_{1-x}Mn_x$ thin films, tadpole shaped clusters can be observed in Fig. 1(b)–(d). The higher the Mn concentration, the higher the density of the tadpole shaped clusters can be developed. In order to determine whether tadpole shaped clusters exist in S70-1, extensive TEM investigations were conducted and such clusters are hardly observed in S70-1. To understand the nanostructures of these

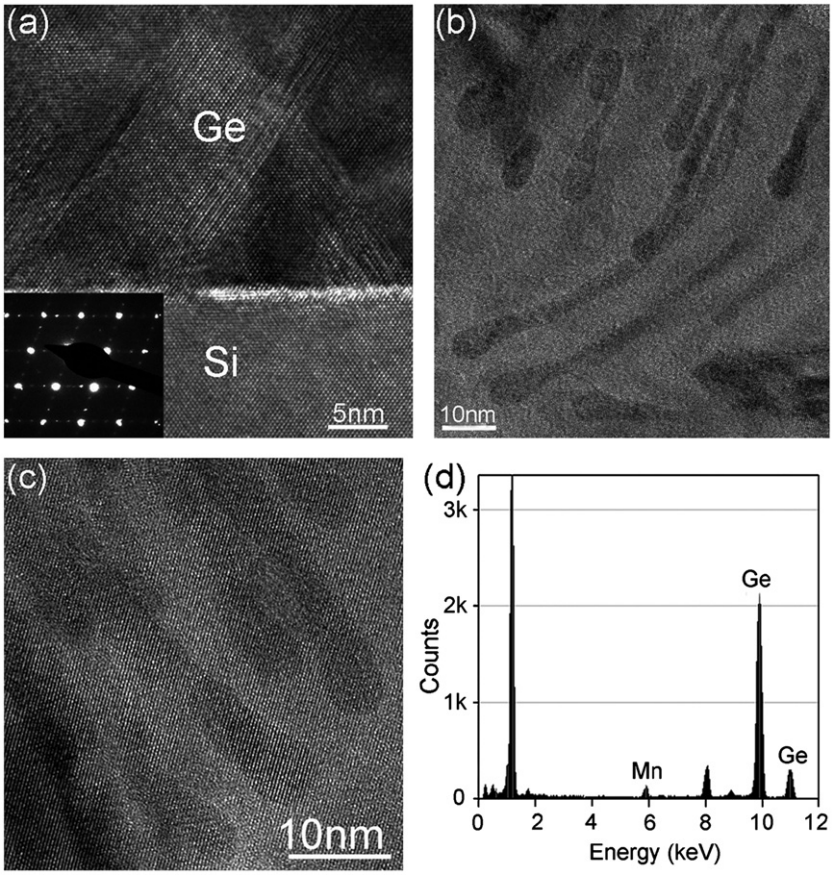

Fig. 2. (a) is a typical HRTEM image of the interface between Ge and Si; (b) shows a high magnification TEM image of the tadpoles; (c) is the HRTEM image and (d) is a EDS profile, showing Mn peaks.

$Ge_{1-x}Mn_x$ thin films, especially the $Ge_{1-x}Mn_x$/Ge and Ge/Si interfaces, HRTEM was employed and a typical $<1\,1\,0>$ zone-axis HRTEM image taken from the interface between the Ge buffer layer and the Si substrate is shown in Fig. 2(a). From the HRTEM image, well epitaxial single-crystalline Ge grown on Si can be clearly seen, although stacking faults stemming from the interface are also observed, due to the large mismatch (~4%) between Ge and Si. The nature of the stacking faults can also be confirmed by the selected area electron diffraction pattern, [9] as shown in the inset of Fig. 2(a). In fact, our extensive HRTEM showed that although a large number of stacking faults interacted within Ge buffer layer, [14] some stacking faults still penetrated the entire film, which may be responsible for the rough surface (refer to Fig. 1). Fig. 2(b) shows a typical high magnification TEM image, which reveals randomly distributed tadpoles within S70-3 and S70-4. Although these Mn-rich tadpoles are not well aligned along the growth direction $[1\,0\,0]_{Ge}$ possibly due to the rough surface induced by the stacking faults, their tails are surprisingly towards the surface of the thin film. This may indicate that there are particular directions (all towards the surface) for Mn diffusion at a certain circumstance during the growth of $Ge_{1-x}Mn_x$ thin films. To identify the nanostructures of these tadpoles, HRTEM images were acquired and a typical example is shown in Fig. 2(c). The Mn-rich tadpoles are verified having an identical structure of the diamond structured Ge matrix, indicating coherent Mn-rich clusters in Ge matrix [12,13]. Quantitative EDS (Fig. 2(d)) confirms an average 4.2% Mn concentration for sample S70-4, which is consistent with the nominal amount (4%). It should be noted that although Mn-rich tadpoles dominate the thin films in S70-3 and S70-4, Mn-rich secondary precipitates, such as Mn_5Ge_3, can still be occasionally observed, [14] agreeing with the results reported by Ahlers et al. [9] where a few Mn_5Ge_3 precipitates together with coherent, cubic structured clusters were observed in 5% Mn-doped Ge grown at 70 °C.

Compared with their counterparts grown at 70 °C, the samples grown at 150 °C show relative smooth surfaces, as presented in Fig. 3(a)–(d), typical cross-sectional TEM images of S150-1, S150-2, S105-3, and S150-4, respectively. This may be due to the fact that at higher temperature growth, adatoms can be more mobile on the growth front that leads to the smooth surface. Furthermore, unlike the case of S70-1, tadpoles as well as Mn_5Ge_3 precipitates can be observed in S150-1 [refer to Fig. 3(a)], which is similar to the case of S70-4 despite the density of tadpoles in S150-1 is low. This implies that growth temperature as well as Mn concentration can impact the formation of Mn-rich secondary precipitates. When Mn concentration or growth temperature reaches a threshold, such Mn-rich secondary precipitates may be formed. In fact, these two influential factors are not independent to each other. High growth temperature usually promotes a fast Mn diffusion, which leads to more Mn available for the nucleation of secondary precipitates, which can be altered by providing a higher Mn concentration in the system but the growth is remained in a relevantly low temperature. In addition, with increase in the Mn concentration, the shape of the Mn-rich clusters changes from tadpoles to round and their sizes become larger, as clearly shown in Fig. 3(d) where the Mn concentration reaches 4%. Also, the density of the secondary precipitates is increased significantly, as evidenced in Fig. 3 and by our extensive HRTEM observations (not shown here). In contrast to the case at 70 °C, Mn-rich secondary precipitates such as Mn_5Ge_3 and $Mn_{11}Ge_8$, other than coherent tadpoles, become dominant in the thin films grown at 150 °C. This is simply because the higher growth temperature and/or higher Mn concentration promote/promotes the nucleation of secondary precipitates more favorably. An example of a typical $Mn_{11}Ge_8$ precipitate is shown in Fig. 4(a), where a HRTEM image was taken along the [0 0 1] zone

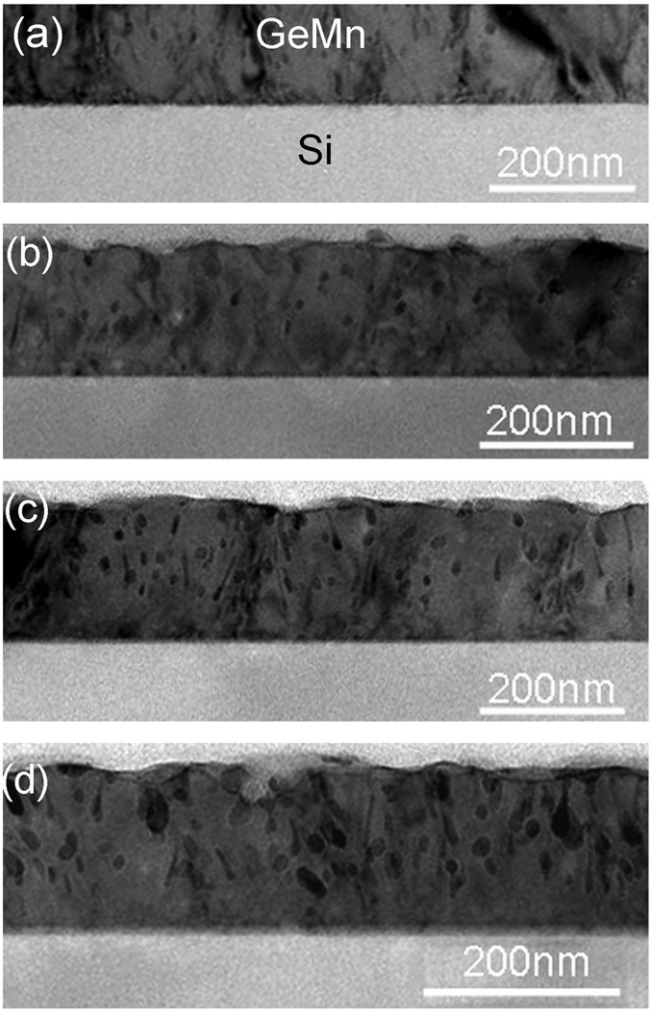

Fig. 3. Typical TEM images of samples grown at 150 °C: S150-1 (a), S150-2 (b), S150-3 (c) and S150-4 (d).

axis of the $Mn_{11}Ge_8$ precipitate [12]. Fig. 4(b) shows a magnified Fourier filtered image [22] of the marked area in Fig. 4(a). Two sets of perpendicular atomic planes (with spacings of 0.33 and 0.26 nm) on the right-top corner of Fig. 4(b) match well with {4 0 0} and {0 2 0} atomic planes of the orthorhombic $Mn_{11}Ge_8$. [12] It has been reported that hexagonal Mn_5Ge_3 precipitates usually have a well-defined orientation relationship with the Ge matrix as $[0\,0\,0\,1]_{Mn5Ge3}//[0\,0\,1]_{Ge}$ and $[\bar{2}\,1\,1\,0]_{Mn5Ge3}//[1\,1\,0]_{Ge}$. [10,17] For orthorhombic $Mn_{11}Ge_8$, however, no particular crystallographic orientation with respect to the Ge matrix has been established. Nevertheless, it is worthwhile to mention that the spacing of {4 0 0} atomic planes of $Mn_{11}Ge_8$ is almost identical to that of {1 1 1} atomic planes of Ge matrix, which might result in a particular crystallographic relationship between Ge matrix and the $Mn_{11}Ge_8$ precipitates. This speculation is indeed confirmed by our HRTEM investigation, as displayed in Fig. 4(b). The image shows that the {1 1 1} planes of Ge are parallel to the {4 0 0} planes of $Mn_{11}Ge_8$, however, for other primary crystallographic directions, there is no particular orientation relationship between Ge matrix and $Mn_{11}Ge_8$ precipitates.

3.2. Magnetic properties

The magnetic properties of the $Ge_{1-x}Mn_x$ thin films were measured by SQUID. Typical temperature-dependent magnetization

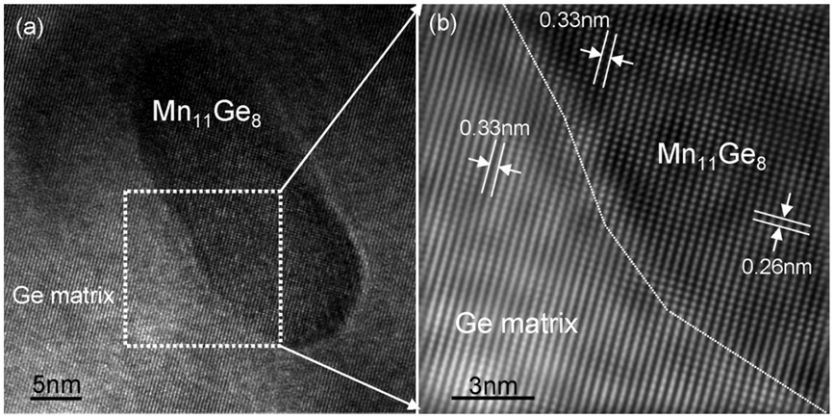

Fig. 4. (a) is a typical HRTEM image, showing a $Mn_{11}Ge_8$ cluster and (b) shows the Fourier filtered image of the marked area in (a).

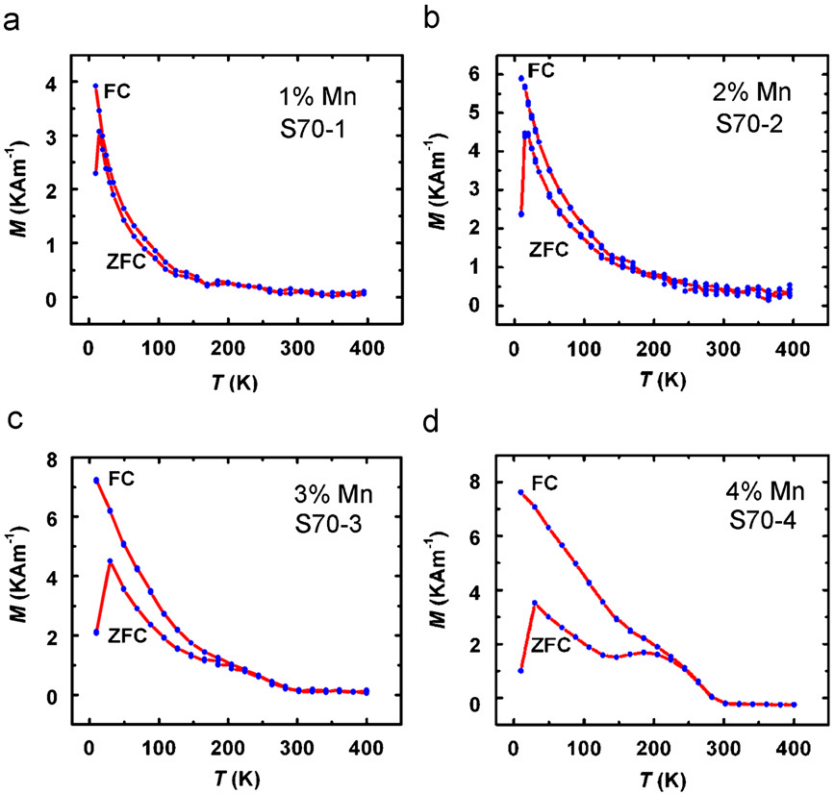

Fig. 5. ZFC and FC curves measured with a magnetic field of 200 Oe for samples S70-1 (a), S70-2 (b), S70-3 (c) and S70-4 (d).

in zero-field cooled (ZFC) and field cooled (FC) conditions for all grown samples are shown in Fig. 5 (grown at 70 °C) and 6 (grown at 150 °C), respectively. Practically, to acquire ZFC curves, samples were firstly cooled under the zero magnetic field from 350 to 10 K, and subsequently measured the magnetic moments while the samples were warmed up under a magnetic field of 200 Oe. For the FC curve acquisition, however, samples were cooled with an applied magnetic field of 200 Oe. By examining the difference between these ZFC and FC curves, the phase transformation, the blocking temperature (T_b), and the Curie temperature (T_c) of the $Ge_{1-x}Mn_x$ thin films can be estimated. For the samples grown at 70 °C, a magnetic transition at around $T_b=22$ K, as a common characteristic, can be clearly observed in Fig. 5. We attribute this transition to the blocking of coherent Mn-rich tadpoles. As mentioned earlier, coherent tadpoles were observed in S70-2, S70-3, and S70-4. Although no tadpoles were seen in S70-1, the ZFC and FC investigations indicate the existence of such coherent clusters. In fact, our result is consistent with the results reported by others who also observed this kind of transition [9,23]. For example, Ahlers et al. [9] explained the transition at $T_b=12$ K as a magnetic behavior of lattice coherent nano-sized clusters. As no other types of clusters were detected in S70-1 and S70-2, these two samples show a paramagnetic behavior above 22 K up to room temperature. On the other hand, with the formation of Mn_5Ge_3 precipitates, S70-3 and S70-4 showed another $T_b=250$ K, as evidenced in Fig. 5(c) and (d), respectively, which is also consistent with the previous results [9,23]. Moreover, the magnetic moment decreases to zero when the temperature increases to room temperature, indicating a T_c of ~300 K. This matches with the well accepted model that the origin of room temperature T_c is associated with the Mn_5Ge_3 precipitates.

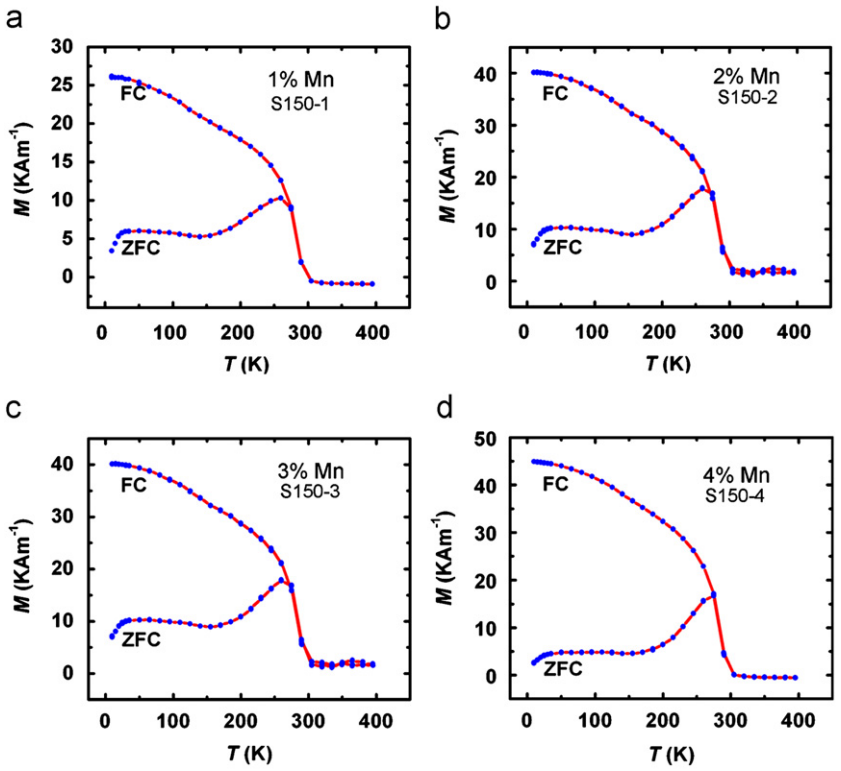

Fig. 6. ZFC and FC curves measured with a magnetic field of 200 Oe for samples S150-1 (a), S150-2 (b), S150-3 (c) and S150-4 (d).

Table 1
Sample details and clustering types.

Samples	T_s (°C)	Mn	Clusters
S70-1	70	1%	Coherent nanoclusters
S70-2	70	2%	Coherent tadpoles start to nucleate
S70-3	70	3%	Tadpoles dominate
S70-4	70	4%	Tadpoles dominate
S150-1	150	1%	Tadpoles and secondary clusters
S150-2	150	2%	Secondary clusters (such as Mn_5Ge_3 and $Mn_{11}Ge_8$) dominate
S150-3	150	3%	Secondary clusters dominate
S150-4	150	4%	Secondary clusters dominate

[9,14,24] As for the samples grown at 150 °C, since all the samples are confirmed with the existence of Mn-rich secondary clusters, such as Mn_5Ge_3 and $Mn_{11}Ge_8$, their ZFC and FC curves are quite similar (Fig. 6) and mainly related to these clusters. In addition, Figs. 5 and 6 show that increase in growth temperature and Mn concentration would systematically enhance the magnetization of the GeMn samples, indicating that both factors are important to control the doping process.

Generally speaking, the magnetic properties of $Ge_{1-x}Mn_x$ thin films grown on Si at both temperatures are closely correlated to their nanostructures (refer to Table 1): since the thin films in S70-1 and S70-2 with low Mn concentration were grown at low temperature, solely magnetic behaviors of coherent nanoclusters are shown. With increase in the Mn concentration (e.g. in S70-3 and S70-4), Mn_5Ge_3 precipitates start to form and the magnetic behaviors show a complex behavior due to the mixture of coherent tadpole shaped clusters and secondary Mn_5Ge_3 precipitates. When the growth temperature rose to 150 °C, secondary precipitates such as Mn_5Ge_3, coexisting with coherent Mn-rich clusters, can be observed even in the 1% Mn-doped Ge thin film (refer to S150-1), which is similar to the case of S70-4. Further increase in the Mn concentration, secondary precipitates dominate the magnetic properties of grown thin films, as evidenced by the variation of the difference for the ZFC and FC curves. The difference becomes the most prominent for the 4% Mn-doped Ge, where the highest density of secondary precipitates can be observed within the entire films, as shown in Fig. 3(d). In this regard, ZFC–FC curves can not only act as a sign of the types of nano-sized clusters/precipitates, but also provide possible information about the amount of different clusters/precipitates in the thin films.

4. Conclusion

In this study, we have systematically investigated the structural and magnetic properties of $Ge_{1-x}Mn_x$ thin films grown on Si substrates using MBE, with different nominal Mn concentrations (1 – 4%) and different growth temperatures by TEM, HRTEM, EDS and SQUID. For the samples grown at 70 °C, coherent Mn-rich clusters were verified to exist even at 1% Mn, and with increase in the Mn concentration, coherent tadpoles dominate the thin films. As for the thin films grown at 150 °C, however, a significant number of tadpoles formed in the film with only 1% Mn. Mn-rich secondary precipitates such as Mn_5Ge_3 and $Mn_{11}Ge_8$ became dominant with increase in the doping concentration. Furthermore, coherent interface between $Mn_{11}Ge_8$ precipitates and Ge matrix was first evidenced. The magnetic properties of the GeMn thin films are confirmed to be closely related to the nature and the amount of Mn-rich clusters/precipitates within these GeMn thin films.

Acknowledgements

The Australia Research Council, the Focus Center Research Program-Center on Functional Engineered Nano Architectonics

(FENA) and Western Institution of Nanoelectronics (WIN) are acknowledged for their financial supports of this project.

References

[1] T. Dietl, H. Ohno, F. Matsukura, J. Cibert, D. Ferrand, Science 287 (2000) 1019.
[2] Y.D. Park, A.T. Hanbicki, S.C. Erwin, C.S. Hellberg, J.M. Sullivan, J.E. Mattson, T.F. Ambrose, A. Wilson, G. Spanos, B.T. Jonker, Science 295 (2002) 651.
[3] F.X. Xiu, Y. Wang, J. Kim, A. Hong, J. Tang, A. Jacob, J. Zou, K.L. Wang, Nat. Mater. 9 (2010) 337.
[4] L. Ottaviano, M. Passacantando, S. Picozzi, A. Continenza, R. Gunnella, A. Verna, G. Bihlmayer, G. Impellizzeri, F. Priolo, Appl. Phys. Lett. 88 (2006) 061907.
[5] J.P. Ayoub, L. Favre, I. Berbezier, A. Ronda, L. Morresi, N. Pinto, Appl. Phys. Lett. 91 (2007) 141920.
[6] T. Devillers, M. Jamet, A. Barski, V. Poydenot, P. Bayle-Guillemaud, E. Bellet-Amalric, S. Cherifi, J. Cibert, Phys. Rev. B 76 (2007) 205306.
[7] R. Tsuchidaa, J.T. Asubara, Y. Jinboa, N. Uchitomi, J. Crys. Growth 311 (2009) 937.
[8] Y.X. Chen, S.S. Yan, Y. Fang, Y.F. Tian, S.Q. Xiao, G.L. Liu, Y.H. Liu, L.M. Mei, Appl. Phys. Lett. 90 (2007) 052508.
[9] S. Ahlers, D. Bougeard, N. Sircar, G. Abstreiter, A. Trampert, M. Opel, R. Gross, Phys. Rev. B 74 (2006) 214411.
[10] Y. Wang, J. Zou, Z.M. Zhao, X.H. Han, X.Y. Zhou, K.L. Wang, J. Appl. Phys. 103 (2008) 066104.
[11] M. Ogawa, X. Han, Z. Zhao, Y. Wang, K.L. Wang, J. Zou, J. Crys. Growth 311 (2009) 2147.
[12] Y. Wang, J. Zou, Z.M. Zhao, X.H. Han, X.Y. Zhou, K.L. Wang, Appl. Phys. Lett. 92 (2008) 101913.
[13] D. Bougeard, S. Ahlers, A. Trampert, N. Sircar, G. Abstreiter, Phys. Rev. Lett. 97 (2006) 237202.
[14] Y. Wang, F.X. Xiu, J. Zou, K.L. Wang, A.P. Jacob, Appl. Phys. Lett. 96 (2010) 051905.
[15] F.X. Xiu, Y. Wang, K. Wong, Y. Zhou, J. Zou, A.P. Jacob, K.L. Wang, Nanotechnology 21 (2010) 255602.
[16] A.P. Li, C. Zeng, K. Van Benthem, M.F. Chisholm, J. Shen, S.V.S. Nageswara Rao, S.K. Dixit, L.C. Feldman, A.G. Petukhov, M. Foygel, H.H. Weitering, Phys. Rev. B 75 (2007) 201201.
[17] C. Bihler, C. Jaeger, T. Vallaitis, M. Gjukic, M.S. Brandt, E. Pippel, J. Woltersdorf, U. Gosele, Appl. Phys. Lett. 88 (2006) 112506.
[18] H. Li, Y. Wu, Z. Guo, P. Luo, S. Wang, J. Appl. Phys. 100 (2006) 103908.
[19] M. Passacantando, L. Ottaviano, F. D'Orazio, F. Lucari, M. De Biase, G. Impellizzeri, F. Priolo, Phys. Rev. B 73 (2006) 195207.
[20] E. Biegger, L. Staheli, M. Fonin, U. Rudiger, Yu.S. Dedkov, J. Appl. Phys. 101 (2007) 103912.
[21] A.P. Li, J.F. Wendelken, J. Shen, L.C. Feldman, J.R. Thompson, H.H. Weitering, Phys. Rev. B 72 (2005) 195205.
[22] Y. Wang, J. Zou, Z.M. Zhao, Z. Hao, K.L. Wang, Nanotechnology 20 (2009) 305301.
[23] C. Jaeger, C. Bihler, T. Vallaitis, S.T.B. Goennenwein, M. Opel, R. Gross, M.S. Brandt, Phys. Rev. B. 74 (2006) 045330.
[24] A. Verna, L. Ottaviano, M. Passacantando, S. Santucci, P. Picozzi, F. D'Orazio, F. Lucari, M. De Biase, R. Gunnella, M. Berti, A. Gasparotto, G. Impellizzeri, F. Priolo, Phys. Rev. B 74 (2006) 085204.